LETTERS
PUBLISHED ONLINE: 27 APRIL 2015 | DOI: 10.1038/NCLIMATE2617
nature climate change

Anthropogenic contribution to global occurrence of heavy-precipitation and high-temperature extremes

E. M. Fischer* and R. Knutti

Climate change includes not only changes in mean climate but also in weather extremes. For a few prominent heatwaves and heavy precipitation events a human contribution to their occurrence has been demonstrated[1–5]. Here we apply a similar framework but estimate what fraction of all globally occurring heavy precipitation and hot extremes is attributable to warming. We show that at the present-day warming of 0.85 °C about 18% of the moderate daily precipitation extremes over land are attributable to the observed temperature increase since pre-industrial times, which in turn primarily results from human influence[6]. For 2 °C of warming the fraction of precipitation extremes attributable to human influence rises to about 40%. Likewise, today about 75% of the moderate daily hot extremes over land are attributable to warming. It is the most rare and extreme events for which the largest fraction is anthropogenic, and that contribution increases nonlinearly with further warming. The approach introduced here is robust owing to its global perspective, less sensitive to model biases than alternative methods and informative for mitigation policy, and thereby complementary to single-event attribution. Combined with information on vulnerability and exposure, it serves as a scientific basis for assessment of global risk from extreme weather, the discussion of mitigation targets, and liability considerations.

Significant trends in temperature and precipitation extremes over the recent decades have been observed[7–10] and attributed to human influence[11–15]. Although none of these extreme events was exclusively anthropogenic in a deterministic sense, climate change has changed their odds, which can be expressed as a change in the fraction of attributable risk (FAR; refs 2,16). The FAR framework has been used to quantify the human influence on the occurrence of individual recent heat waves and dry spells[1–4,17] and heavy precipitation and flooding events[5]. Although the framework is effective, the underlying model experiments often have to be designed specifically for certain events. Thus, the FAR estimates for the 2003 European heatwave are only valid for the observed anomaly over the specific area, but do not apply to a similar event occurring further east. Here we extend the FAR framework from individual observed events to global scales. Thereby we address the question of what fraction of extremes occurring globally is attributable to human influence.

We use the two metrics 'probability ratio (PR)' and FAR (ref. 2), defined as $PR = P_1/P_0$ and $FAR = 1 - (P_0/P_1)$, respectively, where P_0 is the probability of exceeding a certain quantile during the pre-industrial control period and P_1 the probability of exceeding it, for example, in present-day climate (see Methods). In simple words, PR is the factor by which the probability of an event has changed, and FAR indicates the fraction attributable to humans. 'Fraction of events' throughout the text should be interpreted as an anthropogenic contribution to the probability of such events, rather than some events being anthropogenic and some not. We base our estimates on well-defined percentiles of daily temperature and precipitation derived from long pre-industrial control runs of 25 CMIP5 models (see models in Supplementary Table 1).

In response to increasing global temperatures, models project more heavy precipitation days, as illustrated by histograms aggregating daily precipitation (Fig. 1) across Northern Europe and North America (see Methods). The simulated occurrence of heavy precipitation days under present-day warming of 0.85 °C (blue lines) is only slightly higher than in pre-industrial conditions. At a warming of 2 °C (red lines) the probability of the most extreme cases, exceeding the pre-industrial 99.99%-quantile, increases by about a factor of 1.5 to 3 depending on region and model (lower panels). This implies that on average across the area an event expected once every 10,000 days (about 30 years), in pre-industrial conditions, is expected every 10 to 20 years at a 2 °C warming. The wet tail of the precipitation distribution becomes fatter; thus, the PR increases most rapidly for the most intense and rarest events (Fig. 1) at the expense of days with moderate, low or no precipitation. This is consistent with the finding that in some cases mean precipitation decreases (primarily owing to large-scale circulation change), whereas extreme precipitation increases owing to increased water-holding capacity of warmer air[18].

The PR averaged over global land regions is illustrated as a function of global temperature increase (Fig. 2). On average over land, at a global warming of 2 °C the probability of precipitation extremes increases by about 65% for moderate extremes (exceeding the 99.9th percentile—that is, expected once in about three years). This corresponds to a FAR estimate of about 0.39 (see Table 1 for uncertainty range)—that is, at 2 °C warming roughly 40% of the heavy precipitation events worldwide are attributable to warming (Fig. 2c). Owing to a lack of century-long homogeneous daily observations with global coverage, this increase in PR cannot be directly observed. However, we demonstrate that, for the period for which observations are available, the change in precipitation extremes per degree global temperature increase in the CMIP5 multi-model is remarkably consistent with observations (see Supplementary Text and Supplementary Fig. 1) and if anything tends to be somewhat underestimated by the models[14,19]. The observed global temperature increase primarily results from human influence, so that in a two-step attribution the changes in the occurrence of temperature and precipitation extremes are attributable to human influence[2,20]. The FAR increases most strongly for the highest

Institute for Atmospheric and Climate Science, ETH Zurich, Universitätstrasse 16, 8092 Zurich, Switzerland. *e-mail: erich.fischer@env.ethz.ch

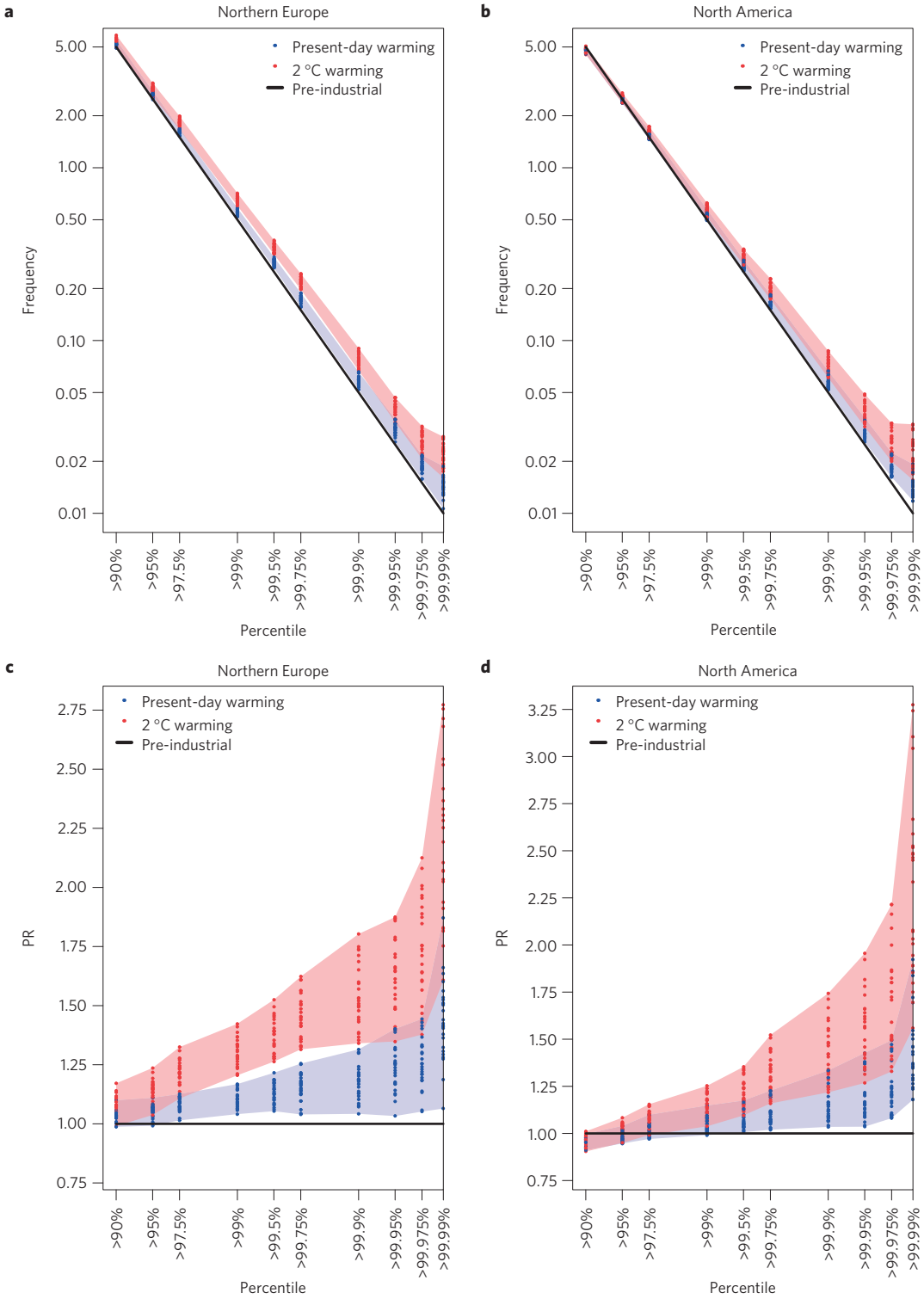

Figure 1 | Regional changes in precipitation extremes. a,**b**, Histograms of daily precipitation for Northern Europe (**a**) and North America (**b**), binned according to the local percentiles in the pre-industrial control simulation (black) of the respective model for a present-day warming of 0.85 °C (blue dots, individual models) and a 2 °C warming (red dots, individual models) relative to pre-industrial conditions. **c**,**d**, Probability ratios (PR) for individual bins relative to pre-industrial conditions for Northern Europe (**c**) and North America (**d**). Bins of all land gridpoints are aggregated across Northern Europe 48°–75° N; 10° W–40° E and North America 12°–66° N; 60°–170° W.

percentiles (Fig. 2c), which implies that particularly the rarest and most extreme heavy precipitation events are attributable to human influence.

The FAR differs substantially between warming targets of 1.5 °C (mean FAR is 0.30, uncertainties given in Table 1), 2 °C (0.39) and 3 °C (0.52). For the observed warming of 0.85 °C, the FAR is about 0.18. This is consistent with the mean FAR (0.19) in the period 1991–2020 even though not all simulations are consistent with the observed warming, which leads to a higher uncertainty range.

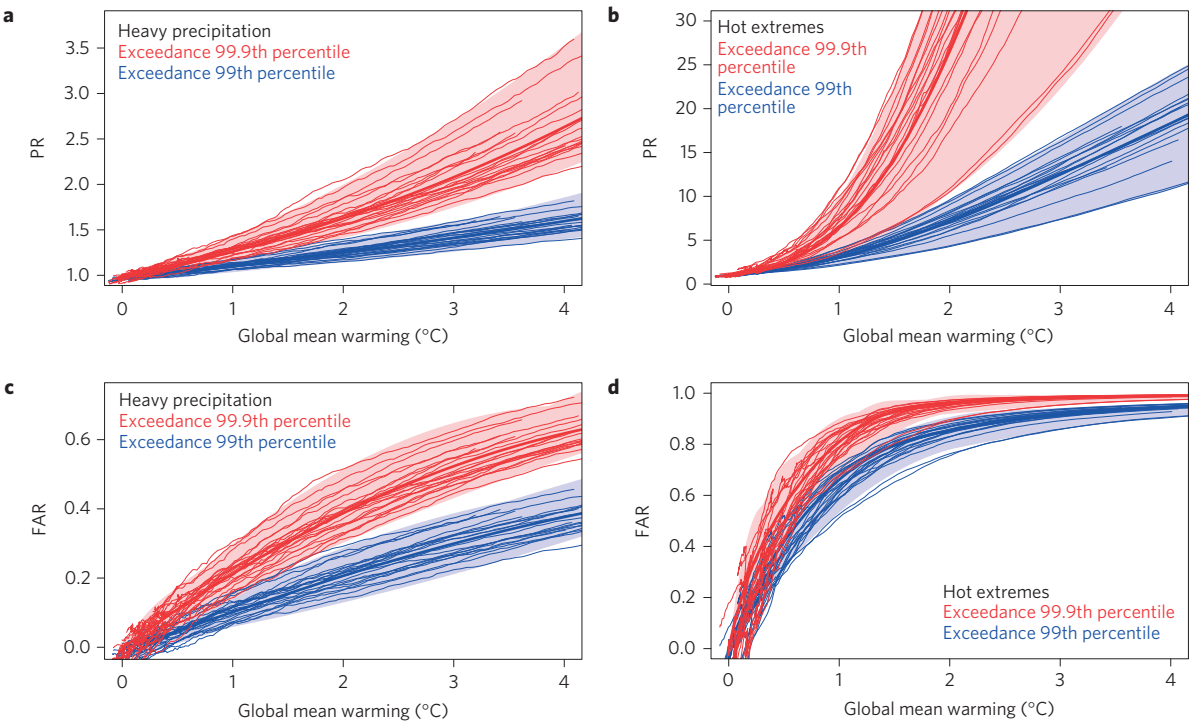

Figure 2 | Rapidly increasing global fraction of attributable risk of extremes over land. a,**b**, Probability ratio of exceeding the (blue) 99th and (red) 99.9th percentile of pre-industrial daily precipitation (**a**) and temperature (**b**) at a given warming level relative to pre-industrial conditions averaged across land. **c**,**d**, Fraction of attributable risk averaged across land for given levels of global warming and selected percentiles for precipitation (**c**) and temperature (**d**).

Table 1 | Model uncertainty in FAR estimates.

Warming	99th percentile	99.9th percentile
Precipitation extremes		
0.85 °C	0.08 (0.03/0.16)	0.18 (0.10/0.28)
1.5 °C	0.15 (0.08/0.24)	0.30 (0.21/0.41)
2.0 °C	0.20 (0.12/0.30)	0.39 (0.29/0.51)
3.0 °C	0.29 (0.20/0.39)	0.52 (0.43/0.64)
Temperature extremes		
0.85 °C	0.60 (0.47/0.66)	0.75 (0.61/0.86)
1.5 °C	0.79 (0.68/0.85)	0.93 (0.84/0.97)
2.0 °C	0.85 (0.78/0.91)	0.96 (0.92/0.99)
3.0 °C	0.91 (0.85/0.94)	0.98 (0.95/0.99)

Multi-model mean estimate and associated minimum and maximum model estimate in brackets for different global warming levels shown in Fig. 2c,d.

In response to increasing global temperatures the PR increases almost everywhere over land and is largest over mid- to high latitudes (see Supplementary Fig. 2 and Table 2) and the tropics, whereas reduced probabilities dominate in subsidence regions off the west coasts (Fig. 3). This pattern is consistent with the multi-model mean changes in precipitation extremes[21–23]. Note that the FAR estimates differ between seasons and regions (Supplementary Table 2).

For temperature extremes, the trend to more hot extremes with increasing global temperature is ubiquitous. Already at an observed warming of 0.85 °C the probability of 1-in-1,000-day hot extremes over land is about five times higher than in pre-industrial conditions—that is, roughly 75% of those moderate hot extremes are attributable to warming (Fig. 2b,d). Again, the CMIP5 multi-model mean agrees well with the observed increase in hot extremes over the past six decades (Supplementary Fig. 1) with a tendency to a slight overestimation in the majority of models[19,24]. The increase in probability and FAR differs across regions (Supplementary Table 3) and is most pronounced over the tropics (Fig. 3) as a result of the weak seasonal cycle and low interannual temperature variability[25,26].

With further warming, the PR of hot extremes increases nonlinearly to very high levels, and the FAR quickly approaches the maximum FAR value ($1 - P_0$). The probability of a hot extreme at 2 °C warming is almost double that at 1.5 °C and more than five times higher than for present-day (Fig. 2b). This result has strong implications for the discussion of different mitigation targets in climate negotiations, where differences between targets are small in terms of global temperatures but large in terms of the probability of extremes.

This nonlinearity is robust and found even for a simple shift of the whole temperature distribution to a warmer climate. We test this by adding the simulated spatial warming pattern consistent with a global mean warming of 2 °C to the entire pre-industrial control run. This yields a similar PR pattern (Supplementary Fig. 3) and remarkably similar global FAR and PR estimates (Supplementary Fig. 4) to the actual transient simulations.

We here focus on daily events, but the probability and FAR of 5-day, 15-day or 31-day temperature and precipitation extremes increase even faster with rising temperatures[27] (Supplementary Fig. 5). For the observed warming the FAR for a 15-day extreme wet spell is about 0.27, compared to 0.18 for daily extremes, and for a 15-day heat wave it is about 10% higher than for daily events, which is consistent with the high FAR estimates and strong increases documented for monthly to seasonal extremes[1–3,10,28]. The primary reason again is that the pre-industrial distribution is narrower for multi-day means or seasonal temperatures than daily temperatures, whereas their mean warming signal is the same.

In a broader context, the approach here is reminiscent of medical studies, where it is not possible to attribute a single fatality from lung cancer to smoking. Instead, a comparison of the lung-cancer-related mortality rate in smokers with the rate in non-smokers may allow attribution of the excess mortality to smoking. Likewise, no single weather event exclusively results from

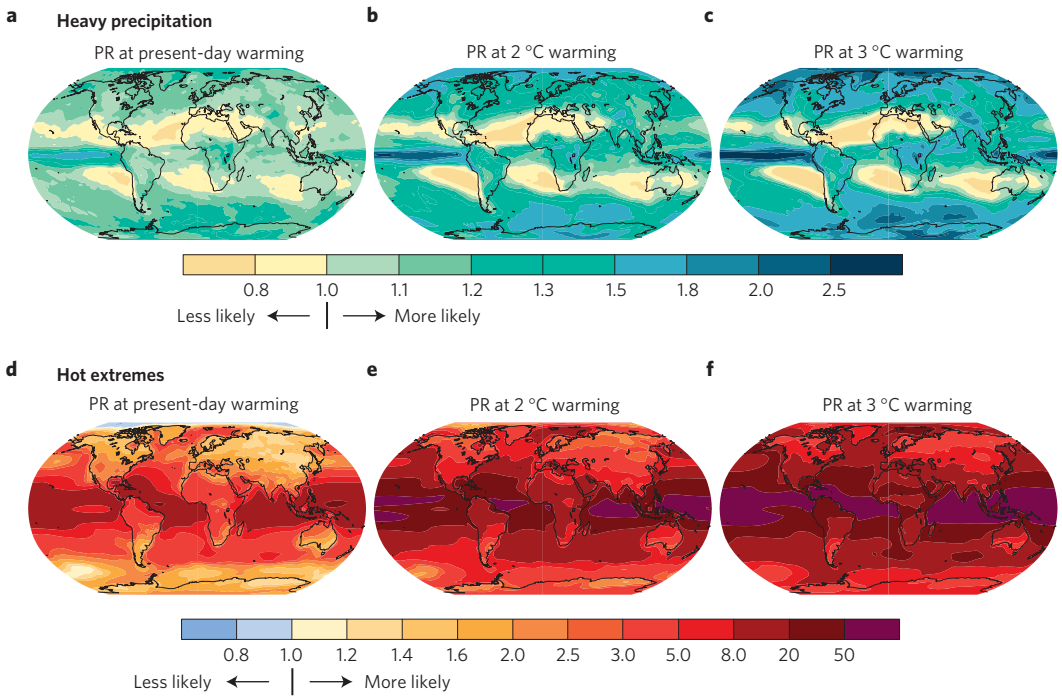

Figure 3 | Change in probability of heavy precipitation and hot extremes. a–f, Multi-model mean probability of exceeding the pre-industrial 99th percentile of daily precipitation (**a**–**c**) and temperature (**d**–**f**), relative to pre-industrial. Ratios are shown for 30-year periods in which the global mean temperatures warmed 0.85 °C (present-day) (**a**,**d**), 2 °C (**b**,**e**) and 3 °C (**c**,**f**) above pre-industrial conditions.

anthropogenic influence in a deterministic sense but arises from complex interactions of atmospheric dynamics, local boundary layer and land-surface interaction and potentially anomalous sea-ice and ocean conditions[29]. Warmer temperatures may influence some of those factors and favour extreme events to happen, and thus the probability of such events increases because of warming.

Quantifying a human contribution to the likelihood of a single event is challenging because there is sometimes a considerable observational uncertainty in the exact intensity of the event, which affects the return period estimate and to a lesser extent also the calculated FAR. Event attribution is based on the assumption that the climate model used can reproduce the observed anomalies during extreme events for the right reason—that is, it provides a reliable representation of the key underlying mechanisms. However, in some cases models may even be unable to simulate the extent of an observed event, which implies that bias correction of mean and possibly even higher-order moments are required[1,4]. We here avoid the problem of observational uncertainty, and reduce the sensitivity to model biases by using percentile thresholds that are well defined from very long control runs. However, model biases in higher-order moments such as variance or skewness may still be relevant. For instance, if a model underestimates the present-day variance or simulates a too negatively skewed temperature distribution, the exceedance probability for a given warming would be overestimated. However, a bias correction of variance and skewness with observational data would potentially induce a high uncertainty given the lack of observational coverage and long temperature series. It should be noted that models have well-known deficiencies in representing some of the driving processes of extremes, such as blocking frequency and persistence, parameterized convection and land-surface feedbacks. Nevertheless, we argue that the changes in probability ratio are robust, assuming that the models accurately capture the patterns of the forced response. The fact that the simulated changes in extremes per degree warming agree with observations, and that our findings are consistent with a mean shift of the distribution, increases our confidence in the estimates. The finding that a substantial fraction of the globally occurring hot and heavy precipitation extremes are attributable to the observed warming is consistent with trend attribution studies for temperature extremes[11–13] and precipitation extremes[14,15], and the argument that all of today's weather events are to some extent affected by a warmer and moister climate[30].

The framework applied here prevents us from tying the attribution statements to specific recent events of which society has experienced the direct consequences. However, the advantage of the global perspective is that the statements are more robust owing to better sampling. At the gridpoint scale, internal variability induces very large uncertainties in changes of the frequency of extremes[19]. We demonstrate that the global aggregation cancels this local noise, as nine realizations of the same model yield very similar global FAR estimates (Supplementary Fig. 6). Aggregation may even compensate some local model differences—induced, for instance, by local surface boundary conditions such as soil and vegetation types, representation of lakes and topography. The use of coupled simulations avoids the need to prescribe sea surface temperatures and the assumption that modes of variability in sea surface temperature remain constant[5]. Because the proposed approach uses well-defined thresholds based on very long control runs, it is relatively insensitive to model biases, accounts for model uncertainties in the response of the coupled climate system, and is robust owing to its large-scale perspective. The approach is complementary to existing event attributions that are powerful for communication and informative for local liability consideration and adaptation decisions. The global framework on the other hand can serve as a valuable tool for global risk assessments, informing mitigation and adaptation decisions. To this end it can be combined with vulnerability and exposure maps to assess not only the event probability, but the actual risk. For instance, the fraction of heavy precipitation and hot extremes attributable to warming is highest over the tropics and many island states, which typically have high vulnerability and low adaptive capacities.

Already today 75% of the moderate hot extremes and about 18% of the moderate precipitation extremes occurring worldwide are attributable to warming, of which the dominant part is extremely likely to be anthropogenic[6]. The fraction increases nonlinearly with further warming such that the probability of hot extremes at 2 °C, for example, is double that at 1.5 °C global warming. With every degree of warming it is the rarest and the most extreme events—and thereby the ones with typically the highest socio-economic impacts—for which the largest fraction is due to human-induced greenhouse gas emissions.

Methods

Methods and any associated references are available in the online version of the paper.

Received 27 November 2014; accepted 18 March 2015; published online 27 April 2015

References

1. Otto, F. E. L., Massey, N., van Oldenborgh, G. J., Jones, R. G. & Allen, M. R. Reconciling two approaches to attribution of the 2010 Russian heat wave. *Geophys. Res. Lett.* **39,** L04702 (2012).
2. Stott, P. A., Stone, D. A. & Allen, M. R. Human contribution to the European heatwave of 2003. *Nature* **432,** 610–614 (2004).
3. Lewis, S. C. & Karoly, D. J. Anthropogenic contributions to Australia's record summer temperatures of 2013. *Geophys. Res. Lett.* **40,** 3705–3709 (2013).
4. Sippel, S. & Otto, F. E. Beyond climatological extremes-assessing how the odds of hydrometeorological extreme events in South-East Europe change in a warming climate. *Climatic Change* **125,** 381–398 (2014).
5. Pall, P. *et al.* Anthropogenic greenhouse gas contribution to flood risk in England and Wales in autumn 2000. *Nature* **470,** 382–385 (2011).
6. Bindoff, N. L. *et al.* in *Climate Change 2013: The Physical Science Basis* (eds Stocker, T. F. *et al.*) Ch. 10 (IPCC, Cambridge Univ. Press, 2013).
7. Donat, M. G. *et al.* Updated analyses of temperature and precipitation extreme indices since the beginning of the twentieth century: The HadEX2 dataset. *J. Geophys. Res.* **118,** 2098–2118 (2013).
8. Perkins, S. E., Alexander, L. V. & Nairn, J. R. Increasing frequency, intensity and duration of observed global heatwaves and warm spells. *Geophys. Res. Lett.* **39,** L20714 (2012).
9. Hansen, J., Sato, M. & Ruedy, R. Perception of climate change. *Proc. Natl Acad. Sci. USA* **109,** E2415–E2423 (2012).
10. Rahmstorf, S. & Coumou, D. Increase of extreme events in a warming world. *Proc. Natl Acad. Sci. USA* **108,** 17905–17909 (2011).
11. Christidis, N., Stott, P. & Brown, S. The role of human activity in the recent warming of extremely warm daytime temperatures. *J. Clim.* **24,** 1922–1930 (2011).
12. Min, S. *et al.* Multimodel detection and attribution of extreme temperature changes. *J. Clim.* **26,** 7430–7451 (2013).
13. Morak, S., Hegerl, G. & Christidis, N. Detectable changes in the frequency of temperature extremes. *J. Clim.* **26,** 1561–1574 (2013).
14. Min, S-K., Zhang, X., Zwiers, F. W. & Hegerl, G. C. Human contribution to more-intense precipitation extremes. *Nature* **470,** 378–381 (2011).
15. Zhang, X., Wan, H., Zwiers, F. W., Hegerl, G. C. & Min, S. K. Attributing intensification of precipitation extremes to human influence. *Geophys. Res. Lett.* **40,** 5252–5257 (2013).
16. Allen, M. Liability for climate change. *Nature* **421,** 891–892 (2003).
17. Massey, N. *et al.* Have the odds of warm November temperatures and of cold December temperatures in Central England changed. *Bull. Am. Meteorol. Soc.* **93,** 1057–1059 (2012).
18. Christensen, J. H. & Christensen, O. B. Severe summertime flooding in Europe. *Nature* **421,** 805–806 (2003).
19. Fischer, E. M. & Knutti, R. Detection of spatially aggregated changes in temperature and precipitation extremes. *Geophys. Res. Lett.* **41,** 547–554 (2014).
20. Christidis, N., Stott, P. A., Zwiers, F. W., Shiogama, H. & Nozawa, T. The contribution of anthropogenic forcings to regional changes in temperature during the last decade. *Clim. Dynam.* **39,** 1259–1274 (2012).
21. Sillmann, J., Kharin, V., Zwiers, F., Zhang, X. & Bronaugh, D. Climate extremes indices in the CMIP5 multimodel ensemble: Part 2. Future climate projections. *J. Geophys. Res.* **118,** 2473–2493 (2013).
22. Kharin, V., Zwiers, F., Zhang, X. & Wehner, M. Changes in temperature and precipitation extremes in the CMIP5 ensemble. *Climatic Change* **119,** 345–357 (2013).
23. Fischer, E., Beyerle, U. & Knutti, R. Robust spatially aggregated projections of climate extremes. *Nature Clim. Change* **3,** 1033–1038 (2013).
24. Zwiers, F., Zhang, X. & Feng, Y. Anthropogenic influence on long return period daily temperature extremes at regional scales. *J. Clim.* **24,** 881–892 (2011).
25. Deser, C., Phillips, A., Bourdette, V. & Teng, H. Uncertainty in climate change projections: The role of internal variability. *Clim. Dynam.* **38,** 527–546 (2012).
26. Fischer, E. M., Oleson, K. W. & Lawrence, D. M. Contrasting urban and rural heat stress responses to climate change. *Geophys. Res. Lett.* **39,** L03705 (2012).
27. Angélil, O. *et al.* Attribution of extreme weather to anthropogenic greenhouse gas emissions: Sensitivity to spatial and temporal scales. *Geophys. Res. Lett.* **41,** 2150–2155 (2014).
28. Diffenbaugh, N. S. & Giorgi, F. Climate change hotspots in the CMIP5 global climate model ensemble. *Climatic Change* **114,** 813–822 (2012).
29. Huntingford, C. *et al.* Potential influences on the United Kingdom's floods of winter 2013/14. *Nature Clim. Change* **4,** 769–777 (2014).
30. Trenberth, K. E. Framing the way to relate climate extremes to climate change. *Climatic Change* **115,** 283–290 (2012).

Acknowledgements

We acknowledge the World Climate Research Programme's Working Group on Coupled Modelling, which is responsible for CMIP, and we thank the climate modelling groups for producing and making available their model output. For CMIP the US Department of Energy's Program for Climate Model Diagnosis and Intercomparison provides coordinating support and led development of software infrastructure in partnership with the Global Organization for Earth System Science Portals.

Author contributions

E.M.F. performed the analysis of the models. Both authors conceived the study and contributed to the writing.

Additional information

Supplementary information is available in the online version of the paper. Reprints and permissions information is available online at www.nature.com/reprints. Correspondence and requests for materials should be addressed to E.M.F.

Competing financial interests

The authors declare no competing financial interests.

Methods

We analyse daily output of historical simulations for the period 1901–2005 as well as future projections forced with RCP8.5 for the period 2006–2100. We use output of 25 CMIP5 models that provide all the necessary output to analyse changes in daily temperature and precipitation extremes (see Supplementary Table 1).

We quantify the probability of exceeding certain percentiles of daily temperature and precipitation. The percentiles are calculated at each individual gridpoint from daily data for the last 200 years of the pre-industrial control simulations, which ensures well-defined levels even for the local 99.99% quantiles. Note that, in contrast to the ETCCDI indices TX90 or TN10, we do not use seasonally varying percentiles but calculate the percentiles based on all days of a 200-yr period. Consequently, the temperature extremes occur during the hottest period and do not include the anomalous warm days of the cold season as for TX90. The same 200-yr pre-industrial control period is used for the reference global mean temperature relative to which the warming targets are defined. For precipitation the percentiles are defined across all precipitation and non-precipitation days of the last 200 years of the pre-industrial control run to avoid a change in the number of wet days affecting the percentile level.

In Fig. 1 we illustrate the change in the occurrence of heavy precipitation days using daily histograms aggregating over Northern Europe and North America. To this end we bin the daily precipitation data for each model according to the above pre-industrial percentiles of the respective model. Note that the bins have the same relative limits but the absolute limits differ across gridboxes. We bin daily precipitation for the 30-yr period in which the respective model shows a mean warming of 0.85 °C (present day) and 2 °C at each grid point. The frequency of days in the 30-yr period falling in each of the bins is then averaged across the area of Northern Europe and North America, respectively. Thereby we derive area-aggregated histograms of daily precipitation shown in Fig. 1.

We here use the two metrics 'probability ratio (PR)' and 'fraction of attributable risk (FAR)' introduced by ref. 2. Probability ratio is defined as $PR = P_1/P_0$, where P_0 is the probability of exceeding a certain quantile during the pre-industrial control period—that is, 0.01 for the 99th percentile—and P_1 the probability of exceeding it in any given period (for example, present-day or at 2 °C warming). The fraction of attributable risk is then defined as $FAR = 1 - (P_0/P_1) = 1 - (1/PR)$. Both PR and FAR were referred to as 'risk' in earlier studies[2,16], but PR is just a ratio of frequencies of occurrence, and in our context does not include any damage, vulnerability or exposure, which are accounted for by comprehensive risk definitions. The term FAR has become common, but is better thought of as which fraction of a series of a particular event can be attributed to external influence.

To calculate a global estimate of PR, we first calculate the frequency of exceeding the 99th and 99.9th percentile at each grid point in each year from 1901 to 2100. We then calculate an area-weighted average across land gridpoints to estimate a global PR—and based on that a global FAR. We then calculate a 30-yr running mean of PR and FAR, which in Fig. 2 is plotted against the 30-yr mean of annual global mean temperatures relative to pre-industrial conditions. Based on this we estimate the PR and FAR value for the 30-yr period when the respective model shows a warming of 0.85, 1.5, 2 and 3 °C. The red band in Fig. 2 is derived by fitting a spline to the each model's PR estimates and showing the highest and lowest model estimate for a certain level of warming. Note that this range simply reflects a model spread that may not necessarily reflect an assessed uncertainty range. The PR and FAR estimates for low warming levels include much variability and need to be interpreted with care. The PR values are calculated on the native model grid, which differs in resolution across the models. However, we find no dependence of the PR and FAR estimates on model resolution.